Monthly Notices
of the
ROYAL ASTRONOMICAL SOCIETY

Mon. Not. R. Astron. Soc. **414,** 1667–1678 (2011) doi:10.1111/j.1365-2966.2011.18502.x

Carbon chemistry in Galactic bulge planetary nebulae

L. Guzman-Ramirez,[1⋆] A. A. Zijlstra,[1] R. NíChuimín,[1] K. Gesicki,[2] E. Lagadec,[3] T. J. Millar[4] and Paul M. Woods[1]

[1]*Jodrell Bank Centre for Astrophysics, School of Physics & Astronomy, The University of Manchester, Manchester M13 9PL*
[2]*Centrum Astronomii UMK, ul.Gagarina 11, 87-100 Torun, Poland*
[3]*European Southern Observatory, Karl-Schwarzschild-Str 2, 85748 Garching, Germany*
[4]*Astrophysics Research Centre, School of Mathematics and Physics, Queen's University Belfast, Belfast BT7 1NN*

Accepted 2011 February 8. Received 2011 February 7; in original form 2010 December 22

ABSTRACT

Galactic bulge planetary nebulae show evidence of mixed chemistry with emission from both silicate dust and polycyclic aromatic hydrocarbons (PAHs). This mixed chemistry is unlikely to be related to carbon dredge-up, as third dredge-up is not expected to occur in the low-mass bulge stars. We show that the phenomenon is widespread and is seen in 30 nebulae out of 40 of our sample, selected on the basis of their infrared flux. *Hubble Space Telescope* (*HST*) images and Ultraviolet and Visual Echelle Spectrograph (UVES) spectra show that the mixed chemistry is not related to the presence of emission-line stars, as it is in the Galactic disc population. We also rule out interaction with the interstellar medium (ISM) as origin of the PAHs. Instead, a strong correlation is found with morphology and the presence of a dense torus. A chemical model is presented which shows that hydrocarbon chains can form within oxygen-rich gas through gas-phase chemical reactions. The model predicts two layers, one at $A_V \sim 1.5$, where small hydrocarbons form from reactions with C^+, and one at $A_V \sim 4$, where larger chains (and by implication, PAHs) form from reactions with neutral, atomic carbon. These reactions take place in a mini-photon-dominated region (PDR). We conclude that the mixed-chemistry phenomenon occurring in the Galactic bulge planetary nebulae is best explained through hydrocarbon chemistry in an ultraviolet (UV)-irradiated, dense torus.

Key words: astrochemistry – circumstellar matter – stars: Wolf–Rayet – planetary nebulae: general – Galaxy: bulge.

1 INTRODUCTION

Planetary nebulae (PNe) are remnants of the extreme mass-loss experienced by asymptotic giant branch (AGB) stars, a phase that occurs during the late stages of evolution of low- and intermediate-mass stars, between 1 and 8 $M_\odot$. The intense mass-loss (from 10^{-6} to 10^{-4} $M_\odot$ yr^{-1}) leads to the formation of a circumstellar envelope made of gas and dust (Kwok 2000). The dust strongly emits in the infrared. After the termination of the AGB, the star rapidly increases in temperature and photodissociates and photoionizes the expanding ejecta.

During the AGB phase, a star may evolve from being oxygen rich to being carbon rich, a change reflected in the chemical composition of the stellar wind. The change occurs when carbon produced by He burning is brought to the surface by processes in the stellar interior, thereby increasing the C/O ratio until it exceeds unity and a carbon star is formed. This is the so-called third dredge-up, which occurs at the end of flash burning in the He shell (Herwig 2005). The process depends on stellar mass: Vassiliadis & Wood (1993) showed the third dredge-up occurs if the core mass of the star $M_{cs} > 1.5\,M_\odot$.

This predicts a clear distinction, with some (lower mass) stars showing oxygen-rich ejecta and some (higher mass) stars carbon-rich ejecta. In the molecular ejecta, the CO molecule locks away the less abundant element, leaving the remaining free O or C to drive the chemistry and dust formation. Oxygen-rich shells are characterized by silicate dust, while carbon-rich shells show polycyclic aromatic hydrocarbon (PAH) emission bands and carbonaceous dust. This dichotomy is indeed by and large observed.

The first evidence for mixed chemistry in post-AGB objects was found when one PN (IRAS 07027−7934), with strong PAH emission bands at 6.2, 7.7, 8.6 and 11.3 μm, was found to also show a 1.6 GHz OH maser line (Zijlstra et al. 1991). Observations made with *Infrared Space Observatory* (*ISO*) uncovered several further cases, where PAH emission in PNe occurred together with emission bands of silicates at 23.5, 27.5, 33.8 and 10 μm, usually found in O-rich shells Waters et al. (1998a,b; Cohen et al. 1999, 2002).

The mixed-chemistry phenomenon has also been seen in the Red Rectangle (Waters et al. 1998b) and in PNe with late Wolf–Rayet-type central stars (Waters et al. 1998a), where it is attributed to

⋆E-mail: lizette.ramirez@postgrad.manchester.ac.uk

the presence of old oxygen-rich material in a circumstellar disc, with the PAHs forming in a more recent carbon-rich outflow. Weak PAH emission has, however, been seen in some clearly oxygen-rich objects, such as NGC 6302 and Roberts 22 (Zijlstra et al. 2001). PAH bands have been detected in S-type AGB stars, with C/O ratios close to, but below, unity (Smolders et al. 2010). Cohen & Barlow (2005) have shown that some PAH emission can occur at C/O ratios as low as 0.6.

Perea-Calderón et al. (2009) showed that the mixed-chemistry phenomenon is widespread among the PNe in the Galactic bulge (GB). Their *Spitzer* observations show that the simultaneous presence of oxygen-rich and carbon-rich dust features is common and is not restricted to objects with late/cool [WC]-type stars. The traditional explanation relating the mixed chemistry to a recent evolution towards carbon star is unlikely for the bulge objects, as these old, low-mass stars are not expected to show third dredge-up and therefore should not show enhanced C/O ratios. The few AGB carbon stars in the bulge do not originate from third dredge-up (Azzopardi, Lequeux & Rebeirot 1988). Different explanations are needed.

In this paper, we investigate two alternative scenarios for the presence of C-rich molecules: PAHs swept up from the interstellar medium (ISM) and *in situ* PAH formation via chemical pathways in oxygen-rich environments. This is performed through the analysis of 40 PNe towards the GB for which *Spitzer* spectroscopy is available. *Hubble Space Telescope* (*HST*) images are available for 22 of these. In Section 2, we present the observations. In Section 3, we present a correlation between the silicate emission and the presence of a torus in the PNe from *HST* images. In Section 4, we present a chemical model that forms long C chains in an O-rich environment, and in Section 5, we discuss these results and present our main conclusions.

2 OBSERVATIONS

Perea-Calderón et al. (2009) uncovered the mixed chemistry in 21 GB PNe, out of a total sample of 26, using *Spitzer Space Telescope* spectra. We retrieved and re-reduced these 21 *Spitzer* spectra. We also included the PN H2-20 from Gutenkunst et al. (2008) and a further 18 PNe in the GB for which we found spectroscopic data in the *Spitzer* archive, yielding a total sample of 40.

All the spectra were taken with the Infrared Spectrograph (IRS; Houck et al. 2004). The spectra cover a range between 5.2 and 37.2 μm by using the Short-Low (SL: 5.2–14.5 μm; $64 < R < 128$), Short-High (SH: 9.9–19.6 μm; $R \sim 600$) and Long-High (LH: 18.7–37.2 μm; $R \sim 600$) modules. The data were retrieved from the *Spitzer* Science Center Data Archive using Leopard. The *Spitzer* IRS Custom Extractor (SPICE) was used to do the extraction of the spectra for each nod position from the 2D images. All spectra were cleaned for bad data points, spurious jumps and glitches, and then they were combined and merged to create a single 5–37 μm spectrum. We did not correct for flux offsets between different wavelengths ranges, but these are minor. Offsets can be caused by the fact that the different wavelength ranges use different slits, and our objects have sizes similar to or larger than the slit widths.

22 of the objects were included in an *HST* snapshot survey of 37 GB PNe (proposal 9356, PI Zijlstra). The Wide-Field Planetary Camera 2 (WFPC2) images were taken in three different filters, Hα, *V*, and [O III], with typical exposure times of 2×100, 60 and 2×80 s, respectively. The objects were placed on the CCD of the Planetary Camera (PC) with a pixel scale of 0.0455 arcsec. Pipeline-reduced images were retrieved. Only the Hα images are used here.

The target selection for the original *HST* observation was based on a catalogued diameter less than 5 arcsec. It included a few objects without a known size. Other than this, the target selection was random among the known PNe in the direction of the bulge. The fact that so many of the *Spitzer* samples were included in the *HST* observations indicates that the *Spitzer* target selection indirectly also made use of the diameter. The *Spitzer* samples were mostly selected based on 12-μm flux. The overlap in selection reflects the brighter infrared emission from compact nebulae.

Very Large Telescope (VLT) UVES echelle spectra were obtained for these 22 objects, using an exposure time of 600 s. The spectra cover the wavelength range from 3300 to 6600 Å, with a resolution of 80 000. These spectra were used to investigate the nature of the central stars, based on the presence of stellar emission lines.

3 RESULTS

3.1 External causes: ISM interaction

As argued above, PAHs could be present in an oxygen-rich environment if they are acquired from the ISM. This can be done by gathering interstellar PAHs through the 'wall' where the expanding nebula collides with the ISM, creating a stationary shock (Wareing, Zijlstra & O'Brien 2007), in which the interaction region is dominated by ISM material. As the bulge PNe have a high velocity dispersion with respect to the ISM, the 'wall' is expected to be close to the nebula and one sided.

To test this model, we checked the spatial location of the PAH emission bands, at 6.2 and 11.3 μm, and compared these to that of the 12.8-μm [Ne II] line. The 12.8-μm [Ne II] emission line comes from the ionized region, so the position of the line traces the position of the PN and is not affected by extinction. On the other hand, if the PAHs have been swept up from the ISM, then their physical position would not be at the same position as the PN (or the [Ne II] for this case), so there should be an offset in their positions. This was done for 40 objects in the sample. The peak of the [Ne II] line and the 11.3-μm PAH feature were measured using the SH part of the spectrum.

In a few cases, we found evidence for an offset. In PN Hb 4, the faint 11.3-μm feature is offset by about 6 arcsec from the [Ne II] 12.80-μm emission. In M2-14, the faint 11.3-μm emission is offset by 4 arcsec from the [Ne II] line. We also found an offset of 2 arcsec between the [Ne II] line and the PAH bands at 11.3 μm in the cases of H1-16, H1-50, H2-20, M1-40 and Cn1-5. These smaller offsets may not be real, as the resolution at the position of the peak of the line and the feature is about 2 arcsec. Hb 4 provides the strongest case for a spatial offset. However, as shown below, it has at best weak evidence for mixed chemistry.

Thus, there are only a few potential cases where interaction with the ISM, or other forms of ISM confusion, may contribute to the PAH features. In the large majority of cases, the dust and PAH features are co-located and centred on the nebula. In these cases, the mixed chemistry is likely to have an internal origin, related solely to the star and its ejecta.

3.2 Internal causes: star and nebula

3.2.1 Spitzer spectra

Table 1 lists the 40 PNe we analysed. We identified both PAH and silicate bands, as listed in the table. PAH bands were seen in

Table 1. GB PNe. Columns (3) and (4) list the identified bands in the IRS spectra. Column (5) lists the peak line flux of the 7.7-μm PAH band. Column (6) indicates whether the star has emission line [WC] or is of weak emission-line (wels) type. The last column indicates whether an *HST* image exists. A * in column (3) indicates that the PAH bands are very faint and may be in some doubt. Mixed-chemistry objects are those unstarred objects which do not have 'none' in column (4) (30 in total).

PN G Name	Name	PAHs (μm)	Silicates (μm)	7.7 μm (mJy)	Central star	*HST* image
008.3−01.1	M 1-40	6.2, 7.7, 11.3	27.5, 33.8	400	wels	No
002.2−09.4	Cn 1-5	6.2, 7.7, 11.3	27.5, 33.8	280	[WC4]	No
356.8+03.3	Th 3-12	6.2, 7.7, 8.6, 11.3	33.8	180		Yes
006.5−03.1	H 1-61	6.2, 7.7, 11.3	27.5, 33.8	150	wels	No
006.4+02.0	M 1-31	6.2, 7.7, 11.3	10, 27.5, 33.8	140	wels	Yes
357.1−04.7	H 1-43	6.2, 7.7, 8.6, 11.3	10, 27.5, 33.8	130	[WC11]	Yes
007.2+01.8	Hb 6	6.2, 7.7, 11.3	27.5, 33.8	120		No
358.7+05.2	M 3-40	6.2, 7.7, 8.6, 11.3	27.5, 33.8	111		Yes
356.5−02.3	M 1-27	6.2, 7.7, 11.3	27.5	100	[WC11]	No
004.9+04.9	M 1-25	6.2, 7.7, 11.3	27.5, 33.8	90	[WC6]	No
359.3−01.8	M 3-44	6.2, 7.7, 11.3	27.5, 33.8	80	[WC11]	No
358.9+03.4	H 1-19	6.2, 7.7, 8.6, 11.3	27.5, 33.8	80		Yes
000.1+04.3	H 1-16	6.2, 7.7, 11.3	27.5, 33.8	80		No
352.6+03.0	H 1-8	6.2, 7.7, 8.6, 11.3	27.5, 33.8	70		Yes
003.1+03.4	Hen 2-263	6.2, 7.7, 8.6, 11.3	23.5, 27.5, 33.8	60		Yes
354.5+03.3	Th 3-4	6.2, 7.7, 8.6, 11.3	10, 27.5, 33.8	60		Yes
359.9−04.5	M 2-27	6.2, 7.7, 11.3	27.5, 33.8	60	[WR4]	No
000.0−06.8	Hen 2-367	6.2, 7.7, 11.3	27.5,33.8	60		No
351.9−01.9	K 5-4	6.2, 7.7, 8.6, 11.3	None	50		Yes
356.9+04.4	M 3-38	6.2, 7.7, 11.3	27.5, 33.8	50		Yes
002.8−01.7	H 2-20	6.2, 7.7, 11.3	27.5, 33.8	40		Yes
006.8+04.1	M 3-15	6.2, 7.7, 11.3	27.5, 33.8	20	[WC5]	Yes
007.5+04.3	Th 4-1	7.7, faint 11.3	10, 27.5, 33.8	20		Yes
358.5−04.2	H 1-46	7.7, 11.3	10, 27.5, 33.8	18		Yes
004.0−03.0	M 2-29	7.7, 8.6, 11.3	None	10		No
355.9+03.6	H 1-9	7.7, 8.6	None	10		No
357.2+02.0	H 2-13	Faint 7.7, 11.3	33.8	8		Yes
001.2+02.1	Hen 2-262	Faint 6.2, 7.7, 8.6, 11.3	33.8	8		No
004.1−03.8	KFL 11	Faint 7.7, 8.6, 11.3	33.8	5		Yes
003.1+02.9	Hb 4	Faint 7.7 and 11.3 (*)	27.5, 33.8	5	[WC4]	No
002.9−03.9	H 2-39	Faint 7.7 (*)	23.5, 27.5, 33.8	1		Yes
006.3+04.4	H 2-18	11.3	33.8	0		Yes
003.6+03.1	M 2-14	Faint 11.3 (*)	27.5, 33.8	0	wels	Yes
356.5−03.6	H 2-27	Faint 11.3 (*)	None	0	[WC11]	Yes
358.5+02.9	Al 2-F	Faint 11.3 (*)	33.8	0		Yes
008.6−02.6	MaC 1-11	Faint 8.6, 11.3	33.8	0		Yes
006.1+08.3	M 1-20	6.2, 8.6, 11.3	None	0	[WC8]	No
005.9−02.6	MaC 1-10	11.3	33.8	0		No
008.2+06.8	Hen 2-260	8.6	None	0		No
359.7−02.6	H 1-40	6.2, 11.3	10, 27.5, 33.8	0		No

all objects, except for five objects where only very faint 11.3-μm/7.7-μm bands and no other features were seen. Silicate emission was seen in 34 PNe. We found evidence for mixed chemistry (both PAH and silicate emission) in 30 PNe, where we exclude those with dubious PAH bands.

Table 1 is in order of PAH strength, where the PAH strength is defined as the peak line flux of the 7.7-μm PAH band. From H2-18 onwards, no 7.7-μm emission feature is detected. The spectra are shown in the leftmost panels of Fig. 1. We only show the short wavelength region (SL and LH) to cover the 10-μm silicate feature and the PAH bands. The vertical red lines indicate the wavelength of PAH bands: 6.2, 7.7, 8.6 and 11.3 μm. Offsets between the different spectral segments are visible in three cases.

Th 3-4 (PN G354.5+03.3), H 1-46 (PN G358.5−04.2), and Th 4-1 (PN G007.5+04.3) show a strong broad-band at 10 μm, interpreted as silicate emission. In all three cases, the peak is shifted to longer wavelengths, beyond 10 μm. In the classification scheme of Sloan & Price (1998), they are of type SE4/5. The 13-μm feature, typically associated with the reddest silicates (SE1-4) in AGB stars, is not present in our objects. Perea-Calderón et al. (2009) show three more objects with silicate emission without PAH features – these also have reddish silicates and are of type SE5-6, without a 13-μm feature. The reddening of the silicate emission may be attributed to large dust grains.

3.2.2 *Emission-line stars*

The rightmost panels of Fig. 1 show the UVES spectra of the spectral region around the strong stellar emission C IV-5800/5811 Å line. This line is an indicator for [WC]-type stars. The *y*-axis scale is the same for all panels, except for two objects with strong emission lines. In the case of H1-43 (PN G357.1−04.7), we show the stellar

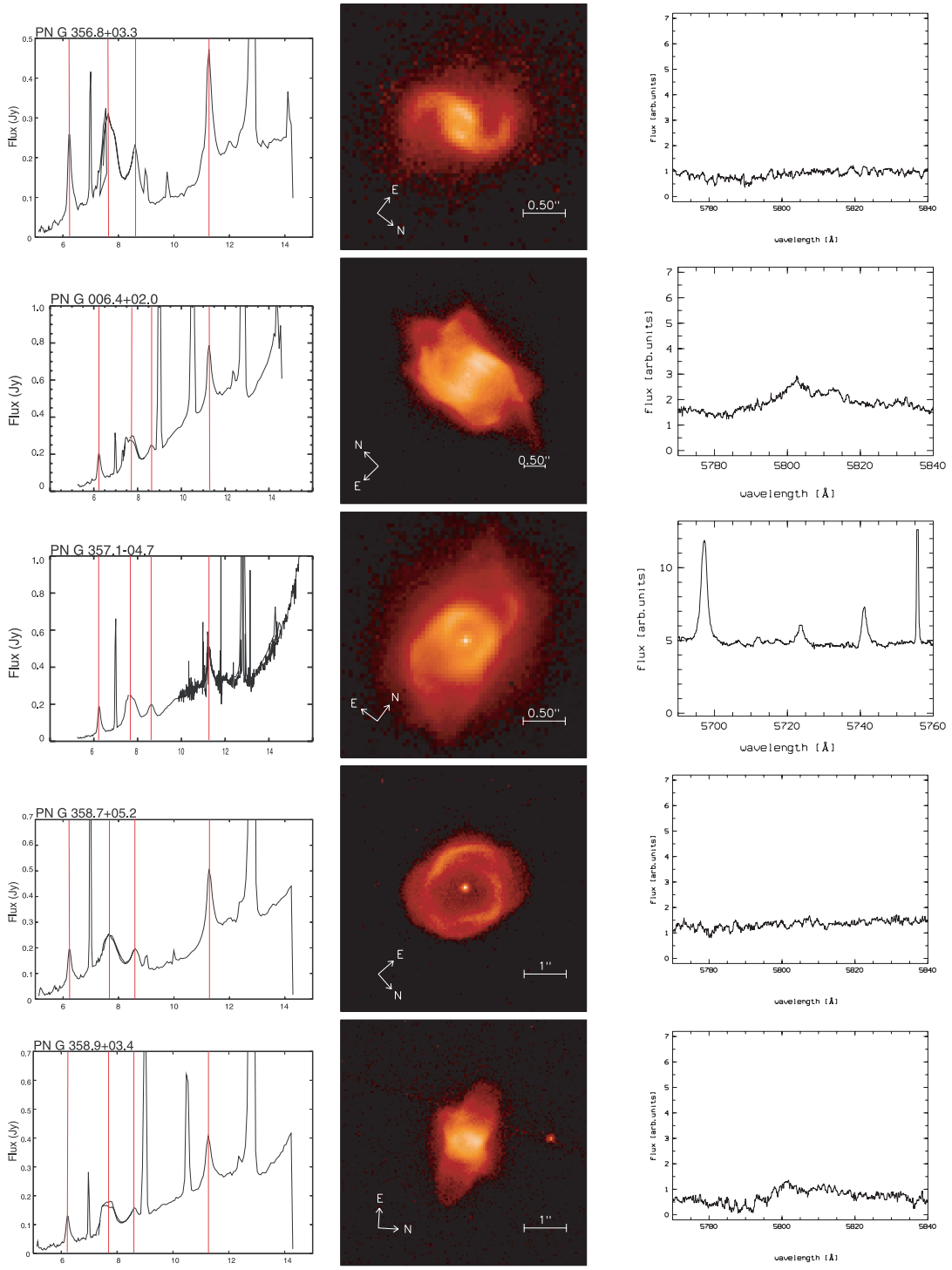

Figure 1. Correlation image showing, in the first column, the 5–15 μm IR *Spitzer* spectrum and the short-wavelength region, and the vertical red lines show the PAH bands. In the second column is the corresponding *HST* image, and in the third column we show a part of the UVES spectrum.

broad line C III at 5696 Å together with the nebular narrow line of [N II] at 5755 Å. The UVES spectra confirm the classification of Górny et al. (2004) but do not reveal any further emission-line stars.

Table 1 shows that the mixed-chemistry phenomenon is not limited to emission-line objects (cf. Górny et al. 2010). In our sample of 30 PNe, 10 have emission-line stars and 20 do not. In the rejected sample of 10 PNe, four have emission-line stars and six do not. This confirms that in the bulge, there is no clear relation between mixed chemistry and class of central star. However, among the mixed-chemistry objects, there is a strong tendency for the emission-line stars to have the strongest 7.7-μm band. Thus, although the mixed chemistry is itself independent of the stellar class, it is amplified by emission-line stars.

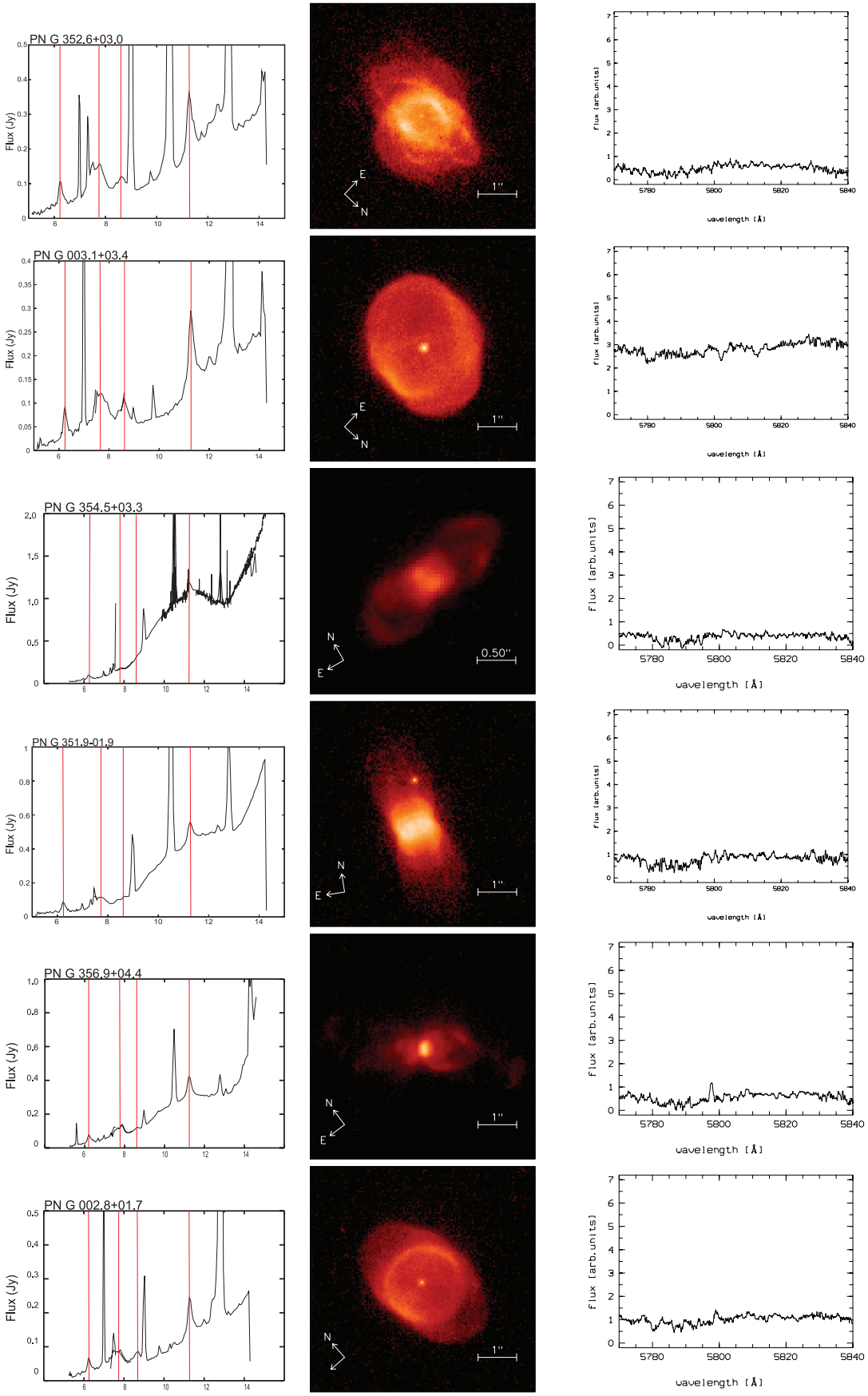

Figure 1 – *continued*

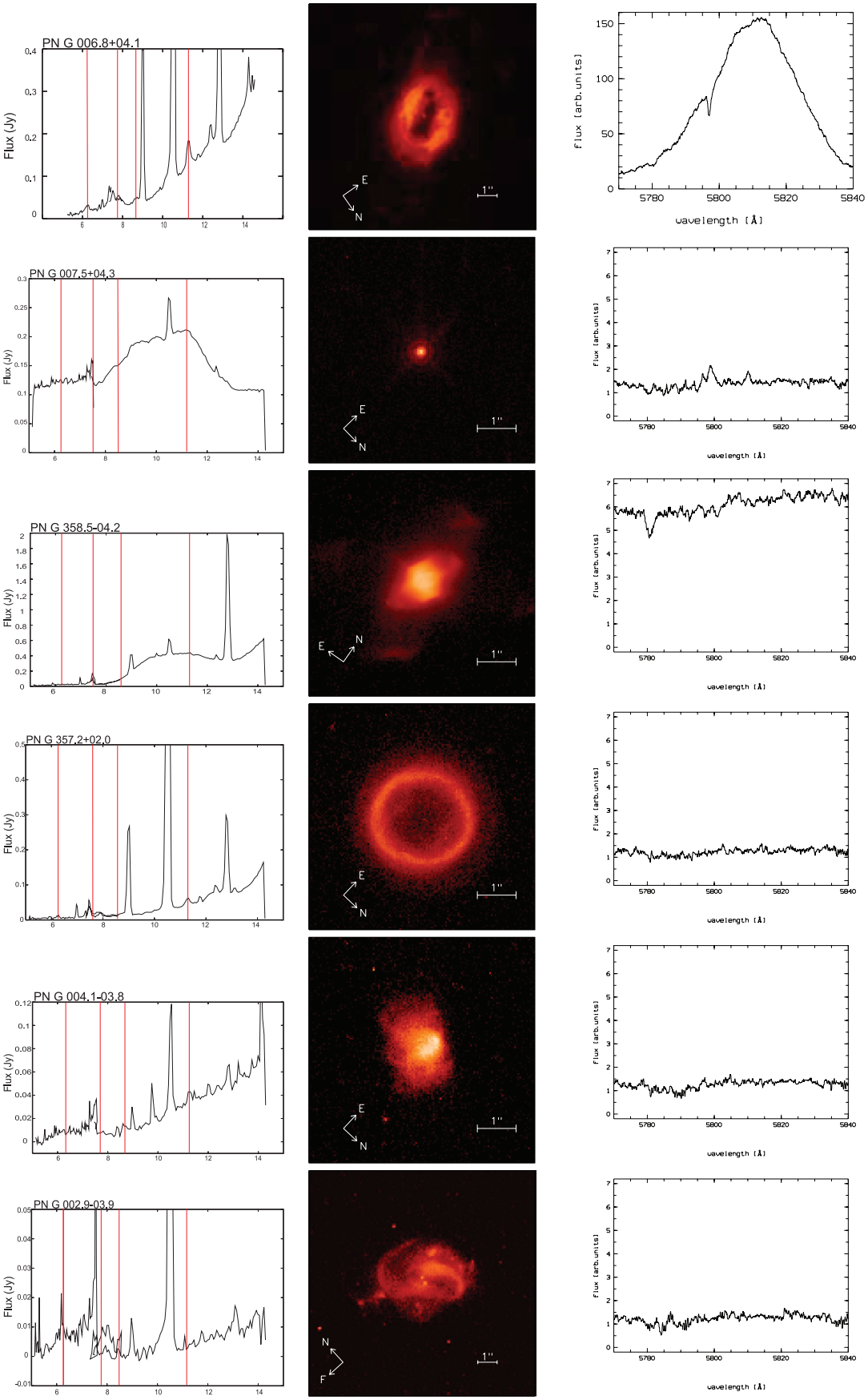

Figure 1 – *continued*

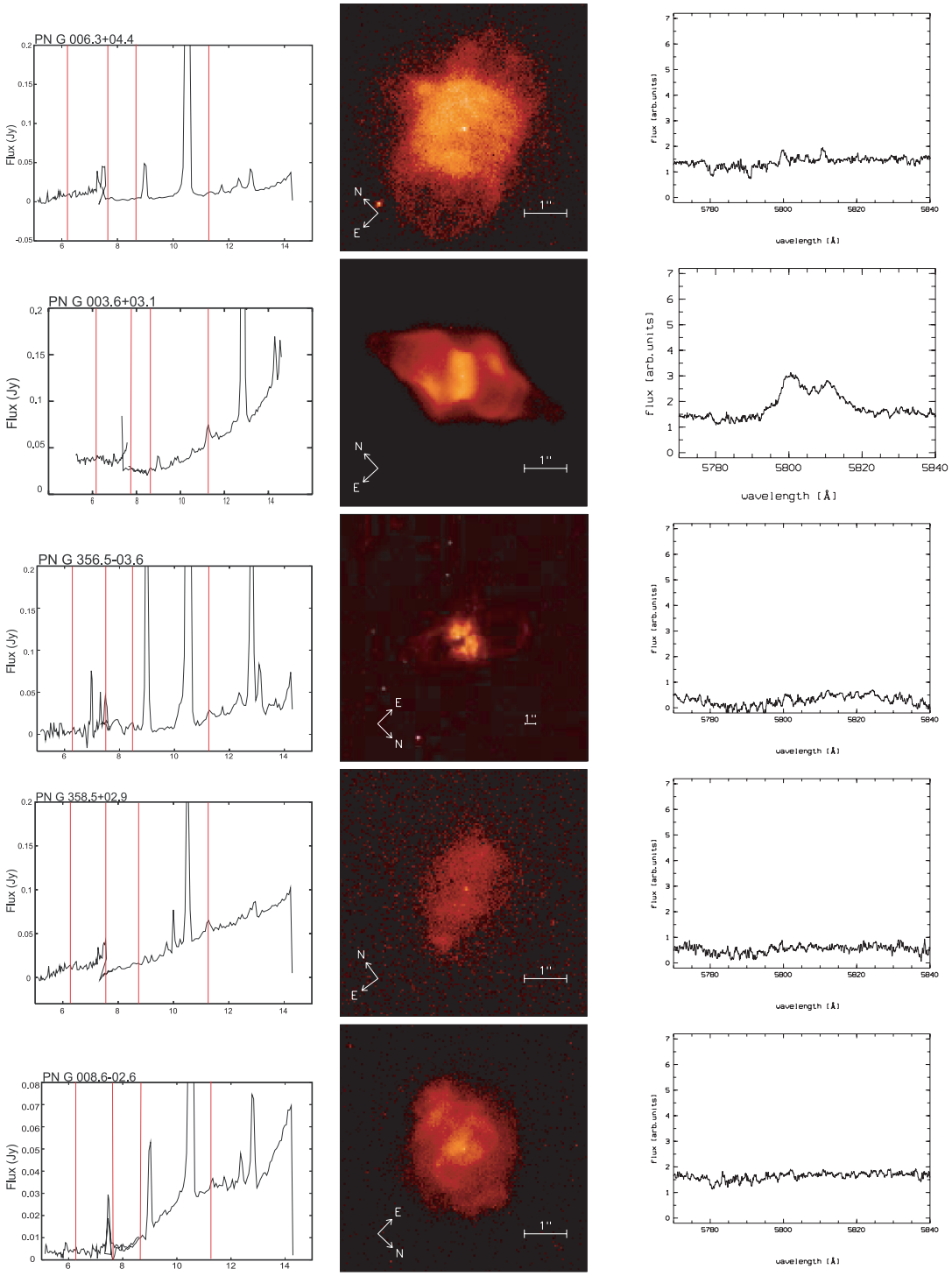

Figure 1 – *continued*

3.2.3 *Morphology*

We use *HST* images of 22 of our objects to study their morphology. The Hα *HST* images are shown in the middle panels of Fig. 1, again in the order listed above (of decreasing PAH strength). The arrows indicate the orientation of the image and the bar indicates the spatial scale. The images are displayed using an 'asinh' scale to enhance the contrast and to better see the faintest structures. (Absolute intensities are not used in this paper.) Note that the images of different objects are not to the same spatial or intensity scale.

A few further images are available in the literature. M1-40 has a diameter of 20 arcsec (Schwarz, Corradi & Melnick 1992) and is therefore likely a foreground nebula. Cn1-5 has a similar-sized halo (Corradi et al. 2003) and also is probably not in the bulge. M1-25 was imaged by Aaquist & Kwok (1990) who find a torus with diameter 1.7 arcsec. Hb 6 and Hb 4 are also not expected to be

in the bulge as their radio fluxes are too high (Zijlstra, Pottasch & Bignell 1989; Aaquist & Kwok 1990).

The most important aspect of Fig. 1 is the predominance of a very specific morphology: a dense torus with bipolar or multipolar flows. This appears to correlate well with the PAH band strength. In a few cases, the torus appears to be seen pole-on (PN G358.7+05.2 and PN G002.8+01.7), but in other cases the structure is easily visible. The confining tori have a range of sizes but are always well defined. The objects without 7.7-μm feature, towards the end of the sequence, tend to show less structured morphologies. The clearest exceptions to the rule are PN G003.6+03.1, which has no 7.7-μm detection (and has a relatively large torus), and PN G003.1+03.4, which does not show elongated lobes, possibly because of viewing angle. We note that one of the three silicate objects (PN G007.5+04.3) is unresolved by *HST* and is extremely compact.

This type of morphology is not the most common in the Galaxy – most PNe are round or elliptical. In the Instituto de Astrofísica de Canarias (IAC) morphological catalogue (Manchado et al. 1996), only 10 bipolar/quadrupolar nebulae are present among 240 objects. Corradi & Schwarz (1995) find that 15 per cent of Galactic PNe are bipolar. Zijlstra (2007) finds 40 per cent of compact bulge PNe are bipolar or related. This is in contrast to our 70 per cent.

We conclude that the mixed-chemistry phenomenon is strongly related to morphology or the presence of a torus. There is no clear relation to the central star, apart from a possible amplification of the PAH bands by emission-line stars.

3.3 Modelling the torus

To test if the dust spectra can be related to the presence of a torus, we model the *Spitzer* spectrum for the representative PN M1-31 (PN G006.4+02.0), using the MC3D (Monte Carlo 3D) program (Wolf, Henning & Stecklum 1999). We did not incorporate PAHs in this model but only used astronomical silicate as the dust component as our aim is to reproduce the shape of the continuum due to emission from these dust grains.

The model has six main parameters that can be adjusted to arrive at the best fit. Other parameters were kept fixed: we used an effective temperature of the star of 57 000 K, a luminosity of 6500 $L_\odot$ (Gesicki & Zijlstra 2007), an inclination of the disc of 90° (edge-on), with the distance to the GB taken as 8.5 kpc (Schneider & Buckley 1996). We did test calculations for a range of inclinations, but found that this parameter has a limited effect on the result, because of the limited opacity at 10 μm of the torus.

The Monte Carlo simulation calculates the radiative transfer for 100 wavelength points between 10^{-3} and 10^3 μm to calculate the dust temperature. It then uses 29 wavelengths between 1 and 53 μm to calculate the spectral energy distribution (SED).

We obtained a best fit for the parameters listed in Table 2. The main parameters are the inner radius of the torus (R_{in}), the outer radius (R_{out}), the dust mass (M_{dust}), the exponent of the power law describing the density in the mid-plane ($r^{-\alpha}$), flaring (r^{β}) and the scaleheight at 100 au from R_{in}, (h_0) (Wood et al. 1998). The fitted inner radius of the torus, of 5000 au, is in good agreement with that measured from the *HST* image (0.55 arcsec which at 8.5 kpc is 4600 au). In Fig 2, we plot the *Spitzer* spectrum and the MC3D

Table 2. Model parameters for the PN M1-31.

R_{in} (au)	R_{out} (au)	$M_{dust}(M_\odot)$	α	β	h_0 (au)
5000	50 000	5.5×10^{-3}	2.5	2	500

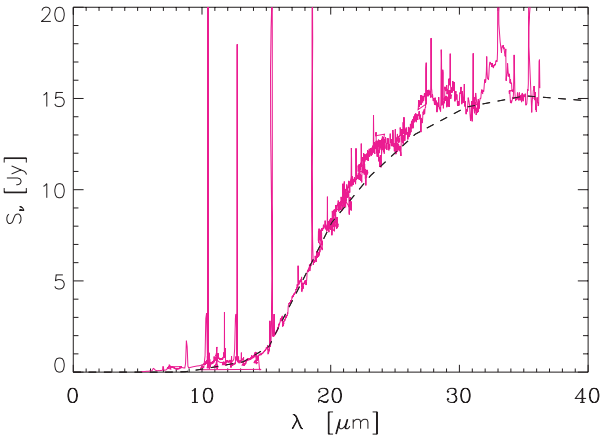

Figure 2. The *Spitzer* spectrum of the PN M1-31. The dashed black line is the model calculated using the MC3D code.

model. A good fit is obtained, with the model reproducing the steep onset of the continuum at 14 μm. The model is a little below the measured flux at shorter wavelengths, which may be due to a contribution from PAH or very small grain continuum emission. We also calculated a model with a mixture of silicate and carbon dust, but it did not reproduce the longer wavelength continuum as well, predicting too much flux longwards of 24 μm.

The inner radius fits the *HST* image well but is relatively far from the star. This indicates that the fitted component is the expanding torus and not a Keplerian disc. The model scaleheight is derived very close to the inner edge of the torus (100 au outside of the inner radius of 5000 au) where it is 10 per cent of the radius, i.e. a thin torus. The flaring increases as r^2, and at the outer edge of the model, the height is equal to the radius. The *HST* image suggests a thickness of the torus which is intermediate between these values. The dust mass indicates a gas mass of around 0.1 $M_\odot$ (for an assumed gas-to-dust ratio of 200) The ionized mass has been estimated as 0.29 $M_\odot$ (Gesicki & Zijlstra 2007). This suggests that the modelled torus accounts for a large fraction of the nebular mass.

Our calculation shows that the dust continuum emission can be explained as arising from the dense torus using oxygen-rich dust (silicate) to explain the SED: there is no significant carbonaceous component. The fitted torus is large and massive. This is a significant finding, as the traditional model for mixed chemistry poses a long-lived, compact oxygen-rich disc. Such a disc is in Keplerian rotation. Waters et al. (1998b) observed in the Red Rectangle a low-mass disc of 500–2000 au in size. Chesneau et al. (2007) observed a disc size of 9–500 au in Mz-3 with a dust mass of 1×10^{-5} $M_\odot$. We do not find evidence for such a component.

In the traditional stellar evolution model, the silicates were ejected $>10^5$ yr ago, with the star subsequently becoming carbon rich prior to the ejection of the main nebula (Habing 1996). In contrast, the torus of M1-31 is part of the main nebula and ejected $<10^4$ yr ago: at this time, the ejecta were oxygen rich. The mixed-chemistry phenomenon is therefore unlikely to be related to the star becoming carbon rich, as the chances of this occurring over such a short timescale are low, whereas the occurrence of mixed chemistry appears to be relatively common.

Interestingly, the two brightest PAH emitters in the mixed-chemistry sample, M1-40 and Cn1-5, are foreground nebulae. These are emission-line stars for which the traditional model of a long-lived disc may hold, similar to objects such as IRAS 07027−7934 and the Red Rectangle. The mixed-chemistry nebulae in the bulge

are a population which is distinct from these disc objects, with a different origin of the mixed chemistry.

4 ORIGIN OF THE PAH IN BULGE PNE

The previous analysis shows that the mixed-chemistry bulge nebulae are likely oxygen rich. This is consistent with expectations based on the stellar population in the bulge. The bulge is believed to contain a 10-Gyr-old population, with little or no trace of younger stars (Zoccali et al. 2003), although recently, some indications have been found for a younger, highly metal-rich population (Bensby et al. 2010).

Carbon stars originate from third dredge-up, which requires a minimum stellar mass of $M_i \gtrsim 1.5\,M_\odot$ (Vassiliadis & Wood 1993). It is not expected to occur in 10-Gyr-old populations. Furthermore, at high metallicity, the formation of carbon stars is inhibited by the large oxygen abundance which needs to be overcome by the primary carbon. Carbon stars are rare in the inner Galaxy (Le Bertre et al. 2003) and absent in the GB (Feast 2007), consistent with this expectation.

This strengthens the case that the mixed chemistry is occurring in oxygen-rich gas expelled by oxygen-rich stars.

We find a strong correlation between mixed chemistry and morphology, specifically, the presence of a massive torus. This indicates that the chemical pathway to the PAH molecules occurs within their high density regions. These tori remain molecular for some time after the ionization of the nebula has started, due to the trapping of the ionization front and due to the shielding effects of the dust column density (Woods et al. 2005). A mini-photon-dominated region (PDR) is expected in these molecular regions (Phillips, Cuesta & Ramos-Larios 2010), slowly being overrun by the advancing ionization front.

A mini-PDR within a dense torus is a plausible location for the PAH formation. In interstellar clouds, PAH emission is often associated with PDR regions (Kassis et al. 2006; Joblin et al. 2010). It is unclear whether PAHs form in these regions or whether they become visible due to ultraviolet (UV) excitation. In our objects, because of the close relationship between morphology and PAHs, it seems likely they form in the regions where they are observed.

In AGB stars, the dichotomy between O-rich and C-rich chemistry can be broken, as is shown by the observation of hot water in the carbon stars IRC +10 216 (Decin et al. 2010; Cherchneff 2011; Neufeld et al. 2011). This may be due to collisional destruction of CO in the shocks (Duari, Cherchneff & Willacy 1999) or interstellar UV photons (Agúndez, Cernicharo & Guélin 2010). The latter authors find that for O-rich circumstellar envelopes, the penetration of interstellar UV photons into the inner layers leads to the formation of molecules such as CH_4 and HCN with abundances relative to H_2 in the range of 10^{-8} to 10^{-7}. This chemistry is initiated by CO dissociation; the dissociation energy of CO is 11.1 eV.

4.1 Chemical reactions

Here we investigate whether a C-rich chemistry can be similarly driven by UV photons penetrating the dense, oxygen-rich torus. The penetration is limited by the dust extinction: in our *HST* image, internal extinction is clearly visible in M3-38 (PN G356.9+04.4) which has the most compact torus.

Our model, which contains gas-phase chemistry only, is based on that of Ni Chuimin (2009) (see also Millar et al. 2007), developed for conditions in PDR regions. It uses an extrapolation of the Meudon 2006 PDR chemistry code (Le Petit et al. 2006) and assumes a semi-infinite and constant-density slab with a density of $2 \times 10^4\,\mathrm{cm}^{-3}$, UV radiation enhanced by a factor of 60 over the average interstellar field, treats thermal balance self-consistently and contains a mixture of reactions extrapolated from the Meudon chemical files and also the UMIST Database for Astrochemistry (UDFA) 2006 (Woodall et al. 2007),[1] Rate 99 (Le Teuff, Millar & Markwick 2000) and Ohio State OSU-03[2] data bases. In Fig. 3, we show the behaviour of the temperature against A_v. As expected, the temperature does not vary much between the three models with each displaying an increase in cooling by atomic O as its abundance increases. Formation and destruction of large hydrocarbon chains, that is with more than four carbon atoms, of the form C_nH_m, ($n \leq 23, m \leq 2$) and their associated ions were added. This resulted in a chemical network of 269 species connected by about 3500 reactions involving ion–neutral and neutral–neutral collisions, photodissociation and photoionization, dissociative and radiative recombination with electrons and radiative association reactions. The goal of the models is to study the abundances of large hydrocarbons. The specific formation of benzene rings (Woods et al. 2002, 2003) and PAHs is not included, but cyclization is assumed to be possible for chains of 23 carbon atoms. Laboratory spectroscopy has shown that this does not yet happen spontaneously for chains of 13 carbon atoms (Giesen 1994).

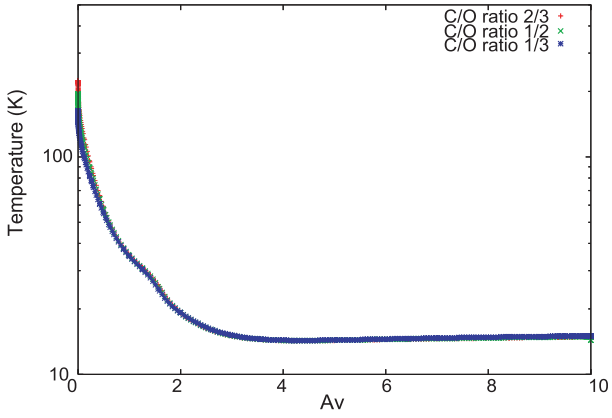

Figure 3. Temperature as a function of visual extinction in our three models. The temperature is calculated self-consistently in the constant-density slab.

The elemental carbon abundance is kept constant at the standard value of 1.32×10^{-4} relative to the total hydrogen abundance (Savage & Sembach 1996), while the elemental oxygen abundance is varied to give a range of C/O values of 2/3, 1/2 and 1/3.

The formation pathways for the carbon chain species in the chemical model include neutral–neutral C atom reactions, radiative association reactions with carbon atoms, and ion–molecule reactions with C^+. Destruction of these chains occurs in reactions with oxygen atoms ($O + C_n$), photodissociation and photoionization, dissociative recombination and electronic recombination reactions (Table 3). The oxygen destruction reaction rates are adopted and extrapolated from the Meudon 2006 chemistry (Le Petit et al. 2006). The oxygen destruction rates for C_2 and C_4 are assumed to be reasonably fast (1.5×10^{-11} and $10^{-10}\,\mathrm{cm}^3\,\mathrm{s}^{-1}$, respectively), while the reaction with C_3 is assumed to have an energy barrier (Woon & Herbst 1996).

[1] http://www.udfa.net
[2] http://www.physics.ohio-state.edu/eric/research.html

Table 3. Example of model reactions of different types.

Oxygen destruction	$O + C_n \rightarrow C_{n-1} + CO$	Meudon
Neutral–neutral	$C + C_nH \rightarrow C_{n+1} + H$	UDFA
Neutral–neutral	$C + C_nH_2 \rightarrow C_{n+1}H + H$	UDFA
Radiative association	$C + C_n \rightarrow C_{n+1} + h\nu$	Meudon
Radiative association	$C + C_nH \rightarrow C_{n+1}H + h\nu$	Meudon
Ion–molecule	$C^+ + C_nH \rightarrow C^+_{n+1} + H$	OSU-03

Example reactions of various types included in the model are listed in Table 3. The last column shows the source of the adopted rate coefficients, either from the Meudon model, the UDFA or OSU-03 data bases.

4.2 Results

If PAH emission does originate from the torus and not from the swept up interstellar gas as is indicated by our observations, then it is valid to consider whether the PAH themselves can be formed in this oxygen-rich, UV-irradiated environment. Since there is no detailed chemical kinetic model for PAH formation, we may use our hydrocarbon chemistry as a proxy for PAH formation, noting that even the presence of abundant hydrocarbons in a PDR would not necessarily prove that PAHs are formed in the same environment.

The PDR model calculations show that the chemistry first tends towards complexity around the C^+/C/CO transition at $A_V \sim 1.4$ mag. This transition is seen in Fig. 4 which plots the abundances of O, C, C+ and CO as a function of A_V. As expected, only O shows a difference between the three models; for the other species, we simply plot the results for the model with C/O = 1/2.

Figs 5, 6 and 7 show the calculated fractional abundances (relative to H_2) for the molecules C_2H, C_8H and $C_{23}H_2$, respectively, as function of A_V, which measures depth into the slab, and C/O ratio.

Two hydrocarbon peaks are seen, one at $A_V \sim 1.5$, and one at $A_V \sim 4$–6. The first peak occurs in the region in which C^+ and H_2 are abundant with the hydrocarbon chemistry initiated by the C^+–H_2 radiative association reaction. Subsequent reactions with C and C^+ form C_2H. C_2H is the main seed molecule for the formation of larger hydrocarbons, as it is in the carbon-rich envelope of IRC+10216 (Millar, Herbst & Bettens 2000), and reactions continue to build up to C_8H, although large(r) hydrocarbons are not highly abundant at low extinction.

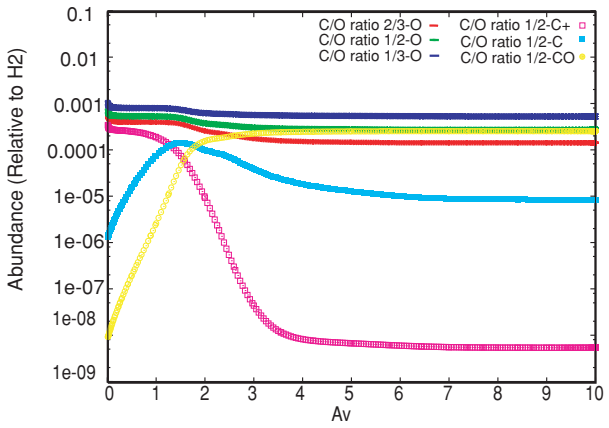

Figure 4. Calculated abundances for O, C, C+ and CO for the three models with varying C/O ratios. Only the O atom abundance varies; other abundances are almost identical in the models and are shown here for the case of C/O = 1/2.

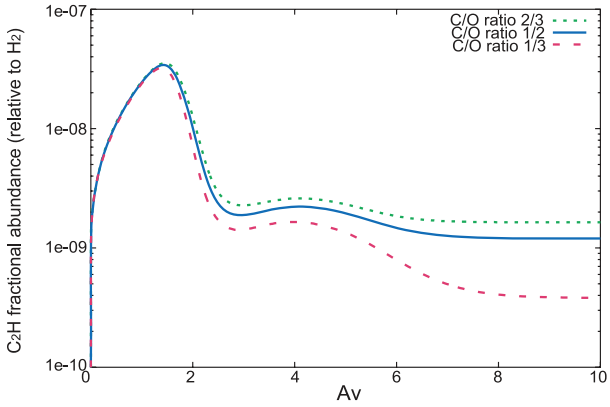

Figure 5. Calculated abundances for varying C/O ratios for C_2H.

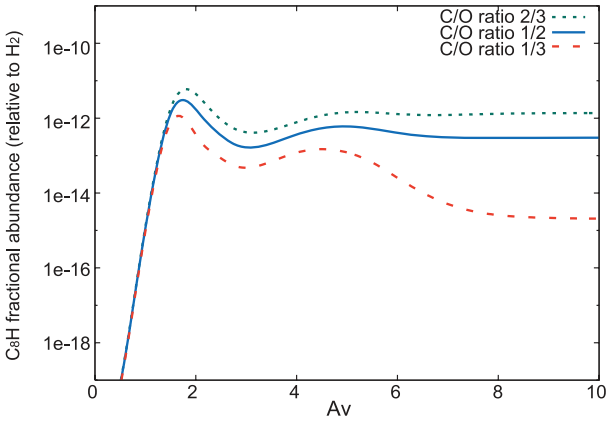

Figure 6. Calculated abundances for varying C/O ratios for C_8H.

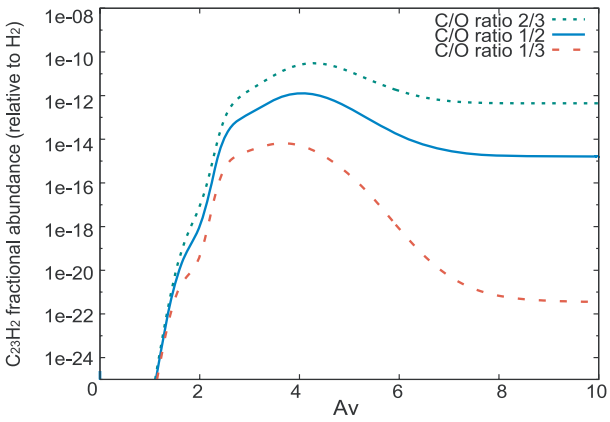

Figure 7. Calculated abundances for varying C/O ratios for $C_{23}H_2$.

The second peak, at higher $A_V \sim 4$–6, occurs where atomic carbon becomes abundant and drives chemistry through proton transfer with H_3^+ to form CH^+ which subsequently reacts with H_2 to form simple hydrides. Here the chemistry produces a surprisingly large abundance of the biggest hydrocarbons in the model.

Oxygen atom destruction reactions are the dominant loss of larger hydrocarbons at high A_V where there is little C^+. The reaction rates of C_2H and C with O are rather uncertain: they differ by an order of magnitude between the UDFA and the Meudon chemical models. However, because of the importance of O, the abundances

depend on the C/O ratios: models with less O produce higher abundances of large hydrocarbons. The difference amplifies for the larger molecules: whereas for C_2H and C_8H, the difference in abundance between C/O = 1/3 and 2/3 is within an order of magnitude, for $C_{23}H_2$ it is 4 orders of magnitude. Even a small increase in the C/O ratio makes a large difference here.

4.3 Discussion

Under the assumptions of the chemical model, it is clear that larger hydrocarbons can form within oxygen-rich environments. It is assumed here that a mechanism exists to convert these long linear hydrocarbon chains into PAH molecules. Such a discovery is surprising, but clues have been previously found in the inner regions of oxygen-rich stars, where small carbon-bearing molecules have been observed, and explained by means of shock chemistry (Cherchneff 2006) or penetration of UV photons Agúndez et al. (2010). Furthermore, in the oxygen-rich environment of a protoplanetary disc, Woods & Willacy (2007) showed that benzene and large polyynes of up to C_8H_2 can form through ion–molecule chemistry in suitably dense conditions, where cosmic ray and X-ray provide a source of ionization. In this latter model, and in the ISM (McEwan et al. 1999), and in proto-PNe with carbon-rich tori (Woods et al. 2002, 2003), closure of the aromatic ring occurs through the reaction of small ($C_{2,...,4}H^{(+)}_{3,...,5}$) hydrocarbons, which are not included in our model due to the simple nature of the Meudon chemistry (Table 3). However, these small hydrocarbons are typically formed by the destruction of larger polyynes, and through reaction with atomic carbon, which are abundant in the chemical model. Once this first aromatic ring closure has occurred, subsequent aromatic growth is rapid in comparison (Cherchneff, Barker & Tielens 1992; Wang & Frenklach 1997).

If we assume that the underlying abundance distribution of hydrocarbon chains is related to that of PAHs, then we can make some inferences on the properties of PAH emission in the GB PNe. First, a reasonable extinction is needed. At low A_V (<2), where carbon is ionized, the abundances of the longest chains are strongly suppressed by photodissociation and photoionization. This still allows for the formation of shorter linear hydrocarbons, but PAH formation is not expected. Efficient PAH formation requires sufficient extinction to render carbon neutral and to minimize the effects of photodestruction. The optimum extinction in our model is around $A_V \sim 4$. At even higher extinction, carbon is locked up in CO and fewer of the longest hydrocarbon chains form, although intermediate chains (C_8H) still form.

In order to generate sufficient reactive C and C^+ UV photons are required to dissociate CO contained in the dense molecular torus. Thus, the central star needs to be hot enough to generate these photons. Our models use a radiation field of 60 times the interstellar radiation field which corresponds to a star of spectral type B, or temperature around 15 000 K. This suggests that the PAHs will not form until the star is hot enough to begin to ionize the nebula. By this time, the nebula will have expanded and the extinction has dropped considerably.

The need for the torus may therefore be to provide an irradiated region dense enough to allow a photon-dominated chemistry in a nebula old enough to allow for an ionizing star. Such a requirement would explain the close relation between PAH emission in oxygen-rich PNe and the presence of a dense torus. This same relation also holds in non-bulge PNe, e.g. NGC 6302 and Roberts 22 (Zijlstra et al. 2001).

The predicted abundances show a strong dependence on C/O ratio (Figs 5, 6, 7). This may explain the finding of Cohen & Barlow (2005) that PAH emission at lower C/O ratio is faint. An increase in the C/O ratio, even if it remains below unity, would benefit PAH formation. But such an increase is not expected in bulge PNe which do not experience carbon dredge-up.

Finally, even though this model goes some way to explaining the observed mixed chemistry, it remains unexplained why PNe with [WC] central stars would have stronger PAH emission. Part of this correlation may be due to the fact that the brightest objects in Table 1 contain some foreground nebulae. However, even excluding these, it still appears that the emission-line stars dominate the top end of the table.

Two possible explanations can be envisaged. First, the stellar winds may inject some carbon into the surrounding nebulae. This would locally enhance the C/O ratio and increase the PAH formation rate.

The second explanation could be related to the energy deposition by the stellar wind into the nebula. Gesicki et al. (2006) show that nebulae around [WC] stars are turbulent indicating that some energy deposition into the nebulae occurs, for instance from the stellar wind. The turbulence may aid in dissociating CO, or more likely, causes compressed regions with a larger range of extinctions. The second explanation appears more plausible. However, the relation between stellar winds and PAH emission needs to be studied further.

We finally note that the A_V in Figs 5–7 and 4 is time dependent. As the torus expands, the extinction drops. The local conditions thus evolve from right to left in the figures. This predicts two layers within the torus, one with the smaller hydrocarbons at $A_V \sim 1.5$ and one with PAHs at $A_V \sim 4$, which are both moving inwards into the torus as the nebula evolves. This makes the layer at lower extinction, with shorter hydrocarbons, a product of the destruction of the PAHs by the increasing UV radiation field. If the PAHs are more UV stable than the largest chains in the model, then PAHs could be present at lower extinction than predicted here.

5 CONCLUSIONS

We summarize the main conclusions of this research in the following list.

(i) We analysed observations of 40 PNe towards the GB using the IRS instrument onboard *Spitzer*. We found that 30 of them present a mixed-chemistry phenomenon. From these 40, we used *HST* observations of 22 to analyse their morphology.

(ii) A strong correlation was found between strength of the PAH bands and morphology, in particular, the presence of a massive torus. Data from VLT/UVES was also used to study their central stars. We find that there is no correlation between the classification of the central star and the mixed-chemistry phenomenon, although PNe with emission-line stars (wels or [WC]) tend to have the stronger PAH emission. This could be related to carbon injection or energy deposition by the wind into the nebula, enhancing PAH formation.

(iii) We modelled the *Spitzer* spectrum for the representative PN M1-31. The SED can be explained using oxygen-rich (silicate) dust. The fitted torus is large and massive, with a size of 5000–50 000 AU au and a mass of 5×10^{-3} $M_\odot$. Because of the age of the torus of M1-31 ($<10^4$ yr), the mixed-chemistry phenomenon is unlikely to be related to a change of composition of the stellar ejecta over time. Such a change would be unexpected in the bulge population (which does not show third dredge-up) and would be very rare over

such a short period in any case, whereas the occurrence of mixed chemistry appears to be relatively common.

(iv) For the chemical analysis of the PAH formation in an oxygen-rich environment, we used the gas-phase models from NíChuimín (2009). These are an extrapolation of the Meudon 2006 PDR chemistry code to include the chemistry of large hydrocarbons. They cover a range of A_V and C/O ratios of 1/3, 1/2 and 2/3. Although the model does not include PAH formation, it shows that large hydrocarbons can form in oxygen-rich environments and that their abundances can be relatively large in moderately shielded regions. The model predicts two layers, one at $A_V \sim 1.5$, where small hydrocarbons form from reactions with C^+, and one at $A_V \sim 4$, where larger chains (and by implication, PAHs) form from reactions with neutral, atomic carbon.

(v) The torus observed in all of the PNe that present the mixed-chemistry phenomenon could provide the dense, irradiated environment needed to form the PAHs detected.

ACKNOWLEDGMENTS

This work is based on observations made with the *Spitzer Space Telescope*, which is operated by the Jet Propulsion Laboratory, California Institute of Technology under a contract with NASA. The VLT/UVES observations are from ESO programme 075.D-0104, and the *HST* images are from the proposal number 9356, PI Zijlstra. LGR and AAZ acknowledge the support of CONACyT (Mexico). Astrophysics at QUB and at Manchester is supported by grants from the STFC.

REFERENCES

Aaquist O. B., Kwok S., 1990, A&AS, 84, 229
Agúndez M., Cernicharo J., Guélin M., 2010, ApJ, 724, L133
Azzopardi M., Lequeux J., Rebeirot E., 1988, A&A, 202, L27
Bensby T. et al., 2010, A&A, 512, A41
Cherchneff I., 2006, A&A, 456, 1001
Cherchneff I., 2011, A&A, 526, L11
Cherchneff I., Barker J. R., Tielens A. G. G. M., 1992, ApJ, 401, 269
Chesneau O. et al., 2007, A&A, 473, L29
Cohen M., Barlow M. J., 2005, MNRAS, 362, 1199
Cohen M., Barlow M. J., Sylvester R. J., Liu X., Cox P., Lim T., Schmitt B., Speck A. K., 1999, ApJ, 513, L135
Cohen M., Barlow M. J., Liu X., Jones A. F., 2002, MNRAS, 332, 879
Corradi R. L. M., Schwarz H. E., 1995, A&A, 293, 871
Corradi R. L. M., Schönberner D., Steffen M., Perinotto M., 2003, MNRAS, 340, 417
Decin L. et al., 2010, Nat, 467, 64
Duari D., Cherchneff I., Willacy K., 1999, A&A, 341, L47
Feast M., 2007, in Kerschbaum F., Charbonnel C., Wing R. F., eds, ASP Conf. Ser. Vol. 378, Why Galaxies Care About AGB Stars: Their Importance as Actors and Probes. Astron. Soc. Pac., San Francisco, p. 479
Gesicki K., Zijlstra A. A., 2007, in Napiwotzki R., Burleigh M. R., eds, ASP. Conf. Ser. Vol. 372, 15th European Workshop on White Dwarfs. Astron. Soc. Pac., San Francisco, p. 41
Gesicki K., Zijlstra A. A., Acker A., Górny S. K., Gozdziewski K., Walsh J. R., 2006, A&A, 451, 925
Giesen J., 1994, High Energy Physics - Theory, preprint (hep-th/9410236)
Górny S. K., Stasińska G., Escudero A. V., Costa R. D. D., 2004, A&A, 427, 231
Górny S. K., Perea-Calderón J. V., García-Hernández D. A., García-Lario P., Szczerba R., 2010, A&A, 516, A39
Gutenkunst S., Bernard-Salas J., Pottasch S. R., Sloan G. C., Houck J. R., 2008, ApJ, 680, 1206
Habing H. J., 1996, A&AR, 7, 97
Herwig F., 2005, ARA&A, 43, 435
Houck J. R. et al., 2004, ApJS, 154, 18
Joblin C. et al., 2010, A&A, 521, L25
Kassis M., Adams J. D., Campbell M. F., Deutsch L. K., Hora J. L., Jackson J. M., Tollestrup E. V., 2006, ApJ, 637, 823
Kwok S., 2000, The Origin and Evolution of Planetary Nebulae. Cambridge Univ. Press, Cambridge
Le Bertre T., Tanaka M., Yamamura I., Murakami H., 2003, A&A, 403, 943
Le Petit F., Nehmé C., Le Bourlot J., Roueff E., 2006, ApJS, 164, 506
Le Teuff Y. H., Millar T. J., Markwick A. J., 2000, A&AS, 146, 157
McEwan M. J., Scott G. B. I., Adams N. G., Babcock L. M., Terzieva R., Herbst E., 1999, ApJ, 513, 287
Manchado A., Guerrero M. A., Stanghellini L., Serra-Ricart M., 1996, The IAC Morphological Catalog of Northern Galactic Planetary Nebulae. IAC, La Laguna, Spain
Millar T. J., Herbst E., Bettens R. P. A., 2000, MNRAS, 316, 195
Millar T. J., Walsh C., Cordiner M. A., NíChuimín R., Herbst E., 2007, ApJ, 662, L87
Neufeld D. A. et al., 2011, ApJ, 727, L28
NíChuimín R., 2009, PhD thesis, Univ. Manchester
Perea-Calderón J. V., García-Hernández D. A., García-Lario P., Szczerba R., Bobrowsky M., 2009, A&A, 495, L5
Phillips J. P., Cuesta L. C., Ramos-Larios G., 2010, MNRAS, 1448
Savage B. D., Sembach K. R., 1996, ARA&A, 34, 279
Schneider S. E., Buckley D., 1996, ApJ, 459, 606
Schwarz H. E., Corradi R. L. M., Melnick J., 1992, A&AS, 96, 23
Sloan G. C., Price S. D., 1998, ApJS, 119, 141
Smolders K. et al., 2010, A&A, 514, L1
Vassiliadis E., Wood P. R., 1993, ApJ, 413, 641
Wang H., Frenklach M., 1997, Combustion Flame, 110, 173
Wareing C. J., Zijlstra A. A., O'Brien T. J., 2007, MNRAS, 382, 1233
Waters L. B. F. M. et al., 1998a, A&A, 331, L61
Waters L. B. F. M. et al., 1998b, Nat, 391, 868
Wolf S., Henning T., Stecklum B., 1999, A&A, 349, 839
Wood K., Kenyon S. J., Whitney B., Turnbull M., 1998, ApJ, 497, 404
Woodall J., Agúndez M., Markwick-Kemper A. J., Millar T. J., 2007, A&A, 466, 1197
Woods P. M., Willacy K., 2007, ApJ, 655, L49
Woods P. M., Millar T. J., Zijlstra A. A., Herbst E., 2002, ApJ, 574, L167
Woods P. M., Millar T. J., Herbst E., Zijlstra A. A., 2003, A&A, 402, 189
Woods P. M., Nyman L., Schöier F. L., Zijlstra A. A., Millar T. J., Olofsson H., 2005, A&A, 429, 977
Woon D. E., Herbst E., 1996, ApJ, 465, 795
Zijlstra A. A., 2007, Baltic Astron., 16, 79
Zijlstra A. A., Pottasch S. R., Bignell C., 1989, A&AS, 79, 329
Zijlstra A. A., Gaylard M. J., te Lintel Hekkert P., Menzies J., Nyman L., Schwarz H. E., 1991, A&A, 243, L9
Zijlstra A. A., Chapman J. M., te Lintel Hekkert P., Likkel L., Comeron F., Norris R. P., Molster F. J., Cohen R. J., 2001, MNRAS, 322, 280
Zoccali M. et al., 2003, A&A, 399, 931

This paper has been typeset from a TEX/LATEX file prepared by the author.